Renewable Energy 99 (2016) 875–887

Contents lists available at ScienceDirect

Renewable Energy

journal homepage: www.elsevier.com/locate/renene

Large-scale experiments on the behaviour of a generalised Oscillating Water Column under random waves

Antonino Viviano [a], Stefania Naty [a], Enrico Foti [a], Tom Bruce [b], William Allsop [c], Diego Vicinanza [d, *]

[a] Department of Civil Engineering and Architecture, University of Catania, Via S. Sofia 64, 95123 Catania, Italy
[b] Institute for Energy Systems, School of Engineering, The University of Edinburgh, Kings Buildings, Mayfield Rd, Edinburgh EH9 3JL, United Kingdom
[c] Coastal Structures Group, HR Wallingford, Howbery Park, Wallingford OX10 8BA, United Kingdom
[d] Dipartimento di Ingegneria Civile, Design, Edilizia e Ambiente, Seconda Universitá di Napoli, Via Roma 29, 81031 Aversa, Caserta, Italy

ARTICLE INFO

Article history:
Received 21 April 2016
Received in revised form
22 July 2016
Accepted 27 July 2016
Available online 3 August 2016

Keywords:
Wave energy converter
Oscillating Water Column
Physical model
Wave reflection

ABSTRACT

This work investigates wave reflection and loading on a generalised Oscillating Water Column (OWC) wave energy converter by means of large scale (approximately 1:5–1:9) experiments in the Grosse Wellenkanal (GWK), in which variation of both still water depth and orifice (PTO) dimension are investigated under random waves. The model set-up, calibration methodology, reflection analyses and loadings acting on the OWC are reported. On the basis of wave reflection analysis, the optimum orifice is defined as that restriction which causes the smallest reflection coefficient and thus the greatest wave energy extraction. Pressures on the front wall, rear wall and chamber ceiling are measured. Maximum pressures on the vertical walls, and resulting integrated forces, are compared with available formulations for impulsive loading prediction, which showed significant underestimation for heaviest loading conditions.

The present study demonstrates that a OWC structure can serve as a wave absorber for reducing wave reflection. Thus it can be integrated in vertical wall breakwaters, in place of other perforated low reflection alternatives. The possibility to convert air kinetic into electric energy, by means of a turbine, may give an additional benefit. Thus the installation of such kind of energy converters becomes interesting also in low energy seas.

1. Introduction

In recent years, wave energy exploitation has seen increasing interest among researchers and government [1–6]. More than 1000 Wave Energy Converters (WECs) have been developed and are patented worldwide [7,8].

One of the main issues for developing these technologies is the economic aspect. Compared to other renewable technologies, WECs costs are, in fact, currently still too high. Furthermore, their development is also heavily dependents upon their reliability and operability in open waters, given that they are exposed to extreme conditions of nature. Critical to their overall expense are the costs of building and/or installing the WEC devices.

A solution to significantly decrease costs would be to develop hybrid devices that can be embedded within coastal or offshore infrastructure. This important new concept for coastal defence structures could make a realistic contribution for the WEC systems to become economically competitive with other renewable energy devices, especially where they can be integrated in existing or expanding structure. Moreover multi-purpose solutions combining renewable energy from the sea (wind, wave, tide), aquaculture and transportation facilities can be considered as a challenging, yet advantageous, way to boost blue growth [9].

Two different types of hybrid breakwaters have been developed over the past decades: caisson Oscillating Water Columns (OWC) [10–19] and rubble mound/sea wall Overtopping Devices [20–24]. In the OWC devices the action of the incident waves induces alternately a compression and an expansion of the air pocket (upper part of the chamber), able to generate an air flow in the air duct connected to the atmosphere. In this duct, a self-rectifying turbine coupled to an electrical generator is driven to produce electrical energy. Overtopping devices generally use a slope facing the waves

* Corresponding author.
E-mail address: diego.vicinanza@unina2.it (D. Vicinanza).

http://dx.doi.org/10.1016/j.renene.2016.07.067
0960-1481/

Nomenclature

δ	thickness of front vertical wall
η	free surface elevation
ω	generic angular frequency
a	draft of front vertical wall
A_0	orifice's cross-sectional area
A_c	chamber's horizontal cross-sectional area
B	longitudinal width of caisson
B_t	transverse width of caisson
C_r	total reflection coefficient of a random wave train
$C_{r(f)}$	spectral reflection coefficient, defined for each wave component of the spectrum
d	water depth from caisson floor
d_0	orifice diameter
f_{In}	complex parameter of nth incident wave component
$F_{n,m}$	complex parameter of the mth probe and nth wave component
f_{Rn}	complex parameter of nth reflected wave component
h	water depth from flume floor
H_s^*	significant incident relative wave height $= H_{m0,i}/h$
h_i	opening height of front vertical wall
h_t	height of caisson chamber
$H_{m0,i}$	significant (spectral) height of incident waves, at the paddle
K	generic wave number
L	generic wave length
L_p	wave length (in depth h) based upon peak period
m	mth probe
n	nth harmonic (wave) component
s	approach slope
s_w	wave steepness
t	time variable
T_p	peak wave period
t_{end}	total duration of data
x	abscissa in the direction of incident wave propagation
x_m	distance between the general probe and the first one

with a reservoir behind to capture the overtopping flows. The energy is extracted via low head hydraulic turbines, using the difference in water levels between the reservoir and the local sea level.

Recently, in a breakwater at Mutriku, 16 OWC chambers were formed in a section of vertical wall [16]. These chambers were however damaged in storms in 2007, 2008 and (most seriously) in 2009. Some of the causes of the damage have been described [17,25]. This failure has particularly demonstrated the need for more research to quantify loadings on and around these devices.

In the context of WECs, OWC devices considered here have the advantage of simplicity, since the only moving part of the energy conversion mechanism is the turbine rotor, which is located above the water level [26]. Despite their relative simplicity, OWC caissons involve complex hydrodynamics as they respond to wave motion. Such a complexity has been highlighted in Ref. [27] by flow visualization experiments, demonstrating that large vortices develop around the front “curtain” wall and internal sloshing occurs during the inflow period. Additionally, internal breakers have been observed indicating that loads on the back wall might be considerably higher than would be anticipated from assumed (pulsating) wave motions.

The flow complexity highlights the importance of analyzing both wave motion and loadings at the OWC caisson. Such analyses were first carried out experimentally by Takahashi [10]. He determined that wave reflections from an efficient OWC device can be relatively small and that its stability against storms is high. Additionally he proposed an analysis method for loads on the caisson, considering the influence of air pressure in the chamber. The incident and reflected wave heights in front of OWC have been investigated experimentally with monochromatic waves in Ref. [28]. The aim of that study was to estimate the rate of conversion of incident wave energy into pneumatic energy (in the air column) and the influence of turbine. The Authors concluded that the energy of the air increases and the reflection coefficient reduces with a turbine. Such results imply some correlation between the wave reflections and the air outflow characteristics. Other experiments, carried out with random waves [29], give values of reflection coefficient in front OWC devices when operating efficiently between $C_r = 0.40$ and 0.54.

OWC hydrodynamics are mainly affected by chamber geometry and turbine pneumatic damping (pressure difference across the turbine). The importance of considering the coupling effect between chamber and air turbine has been investigated in Ref. [30], identifying that the performances of these two elements depend on each other. In particular, the turbine must provide the optimal pneumatic damping in order to achieve (near-)resonant conditions in the chamber. In turn, the chamber must provide the maximum pneumatic energy to maximize energy extraction. The effect of the turbine on air flow inside the chamber is frequently modelled [31] by inserting a restriction (orifice) whose dimensions can be easily varied, so varying the resulting damping.

Evaluation of the loadings induced by waves acting on OWC caisson breakwaters have been reported in Ref. [32], using small scale experiments. In particular, the Authors found that wave pressures on OWC caisson breakwaters are smaller than the wave pressure at vertical wall when compared with the well-known Sainflou [33] and Goda [34] empirical formulas for vertical wall breakwaters. Under the wave conditions tested, it was found that Sainflou's formula [33] overestimated the wave pressures acting on an OWC caisson breakwater; whereas Kuo et al. [32] found that Goda's formula [34] provided good estimation for the horizontal force, but tends to underestimate the overturning moment. Other experiments for estimating wave forces on OWC have been carried out by Ashlin et al. [35], for regular waves. They observed that the peak horizontal wave force acting on the structure can be more than 2.5 to 3 times the peak vertical wave force. Moreover the non-linearity due to the variation in the wave steepness in the case of vertical forces is found slightly more compared to the horizontal forces.

In the present contribution, results of unique large scale tests (at approximately 1:5 to 1:9 of full scale) are presented, in order to give useful information on wave reflection and loadings acting on an OWC breakwater under random waves. Such tests were supported by HYDRALAB IV [36] and were carried out at the Large Wave Channel (GWK) of the Coastal Research Centre (FZK) in Hannover. The details of experimental setup are reported in Section 2. Wave reflection estimation and reflection coefficients as function of OWC geometry and wave conditions are discussed in Section 3. Evaluation of loadings on the structure is presented in Section 4. Finally, Section 5 draws together the conclusions.

2. Experimental setup

The OWC device tested was simply a hollow caisson placed at the top of a short approach slope. All the walls are vertical and the front wall is cut off at the bottom in order to form the chamber opening. A cylindrical duct lead upwards from the roof of the caisson. This duct contains a restriction (i.e. an orifice) which enables the simulation of the damping (power take off, PTO) of an air turbine.

Fig. 1 shows a sketch and photographs of the tested OWC device, with the main parameters of interest. The parameters and the values which have been tested are shown in Table 1, which also distinguishes between fixed and variable dimensions.

The fixed dimensions are those related to the caisson construction and foundation: slope and berm height; longitudinal and transverse width of the internal caisson; height of the caisson; the front vertical wall opening height and its thickness. Model setup parameters varied were the still water depth (h) and orifice diameter (d_0). The variation of the water depth causes the modification of two other linked measures: water depth with respect to the caisson floor (d), and draft or 'curtain wall submergence' of the front wall (a). As the two water levels tested were different by 0.50 m, d and a have two values 0.50 m apart. The orifice diameter, d_0, varies between 0 and 0.3 m, where the zero value corresponds to full closure of the air duct.

Large scale experiments of the described device have been carried out at the Large wave channel (Grosse Wellenkanal, GWK) of the Coastal Research Center, in Hannover. The flume is 307 m long, 7 m deep and 5 m wide and can generate waves having (individual) maximum height of 2 m. The random waves can reach $H_{m0} \approx 1.3$ m.

Table 1
Description of OWC caisson geometrical parameters for both fixed and variable dimensions.

Geometrical parameter	Symbol	Tested value(s)	
Approach slope	s	1:6	Fixed
Height of caisson chamber	h_t	2.30 m	Fixed
Longitudinal width of caisson	B	2.45 m	Fixed
Transverse width of caisson	B_t	1.45 m	Fixed
Thickness of front vertical wall	δ	0.50 m	Fixed
Opening height of the front wall	h_i	1.00 m	Fixed
Orifice diameter	d_0	0–0.30 m	Variable
Water depth from flume floor	h	3.00; 3.50 m	Variable
Water depth from caisson floor	d	1.08; 1.58 m	Variable
Draft of front vertical wall	a	0.08; 0.58 m	Variable

Air compressibility causes scaling issue in OWC small scale physical modelling, as explored by Weber [37]. For these large scale tests, Webers work suggests that the influence of scaling (of chamber height and PTO characteristics) upon device performance will be of the order of 10%. A later paper will compare measurements in small scale tests with these large scale experiments, and include some detailed comparison with Webers predicted influences.

Three OWC caissons were installed across the full width of the flume, with the structure's front face 97.47 m from the wave maker.

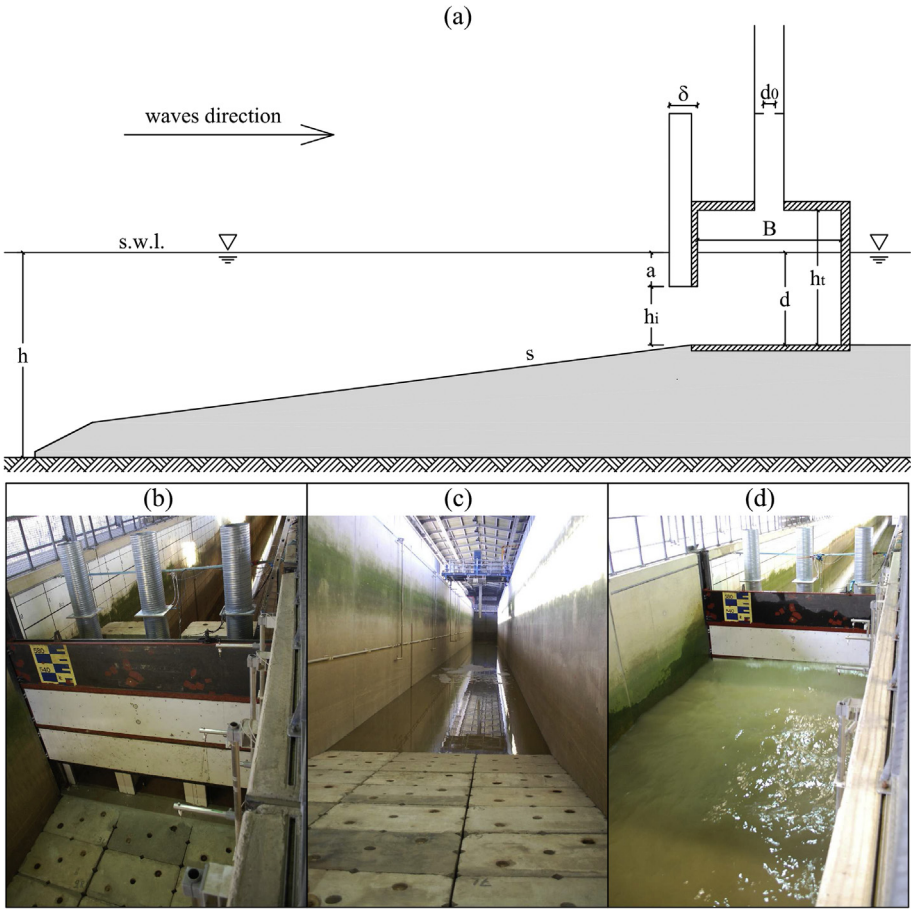

Fig. 1. Schematic representation and photos of OWC caisson tested in the GWK: (a) sketch of the tested configuration with main geometrical parameters; (b) view of front wall and opening; (c) photo of foreshore slope towards the wave maker; (d) view of waves in front of the OWC chambers.

The three OWC caisson were hydraulically identical although only the central one was instrumented. A sketch of the flume arrangement at GWK is shown in Fig. 2, with indication of OWC placement and measurement systems outwith the caisson, in both plan (top) view and longitudinal section. In particular, eight wave gauges have been placed along the flume; four of them (WG01-WG04) have been mounted on the flat bottom full depth zone and they have variable mutual distances in order to be used for evaluating incident and reflected wave components. The other four wave gauges (WG05-WG08) are located near the front wall of the OWC, at intervals of 1 m, with WG08 located 1 m from the wall. Such a packed configuration of near-wall wave probes aims to describe complex wave-structure interactions, also in the presence of breaking waves which may cause impulsive actions. These data have been used in this paper to define the upper limit of the 'wet' domain, in order to compute the forces acting on front wall.

The central caisson was equipped with sensors of different types (see Fig. 3). Five wave gauges (WG09-WG13) allowed measurement of the chamber water surface motion within the OWC chamber. Pressure sensors were installed in a vertical array on the outer side of front wall (P1–P5), on the rear internal wall facing into the chamber (P8–P12), and in the ceiling, again, looking into the chamber (P6, P7, P13). In such a way it was possible to measure pressure distributions, and infer force-time histories, and to identify the most loaded points of the structure. A differential pressure transducer and an air flow propeller were located at the orifice of the duct (the 'chimneys' in Fig. 1(b) and (d)), in order to analyse the air flow characteristics and to relate them to wave reflection and loadings.

The experiments described here were carried out with both regular and random wave conditions. Only random wave tests are analyzed here, since the aim of the present contribution is to study reflection and loadings for an OWC device in realistic sea wave conditions. All the random wave tests, summarized in Table 2, have been carried out using conventional JONSWAP spectra with peak enhancement factor $\gamma = 3.3$. The test matrix of wave height and periods was designed to include tests at the four (nominal) wave steepnesses of $s_w = 0.01$, 0.02, 0.03 and 0.04. This resulted in peak wave periods between 3.0 and 6.5 s; by significant wave heights from 0.26 to 1.00 m (derived as incident wave heights from the reflection analysis). A total of twelve incident random wave conditions at the paddle were tested with the largest water depth of $h = 3.5$ m, five of which were also tested for $h = 3$ m. The wave steepness values of the tested conditions (shown in Fig. 4) are always less than or equal to 0.04.

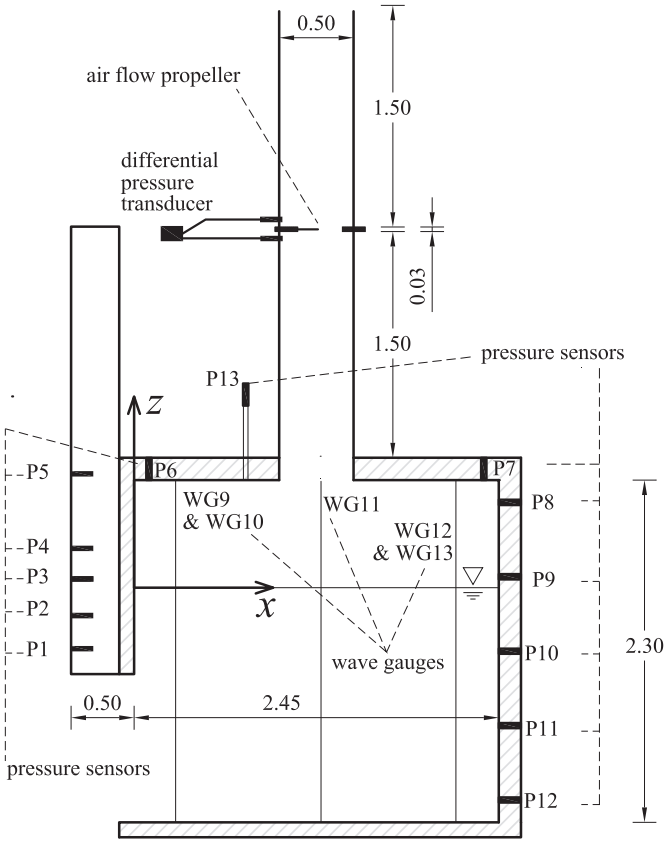

Fig. 3. Detailed longitudinal section of the OWC device with location of measurement sensors and of x and z axes. All dimensions in m.

The full range of the orifice diameter d_0 was explored for only three wave conditions, with different values of T_p and minimum values of h. These tests were performed at the outset, in order to identify an "optimum orifice" which gave the greatest wave energy conversion at the OWC device and, consequently, the least wave reflection. It was established that the "optimum orifice" diameter

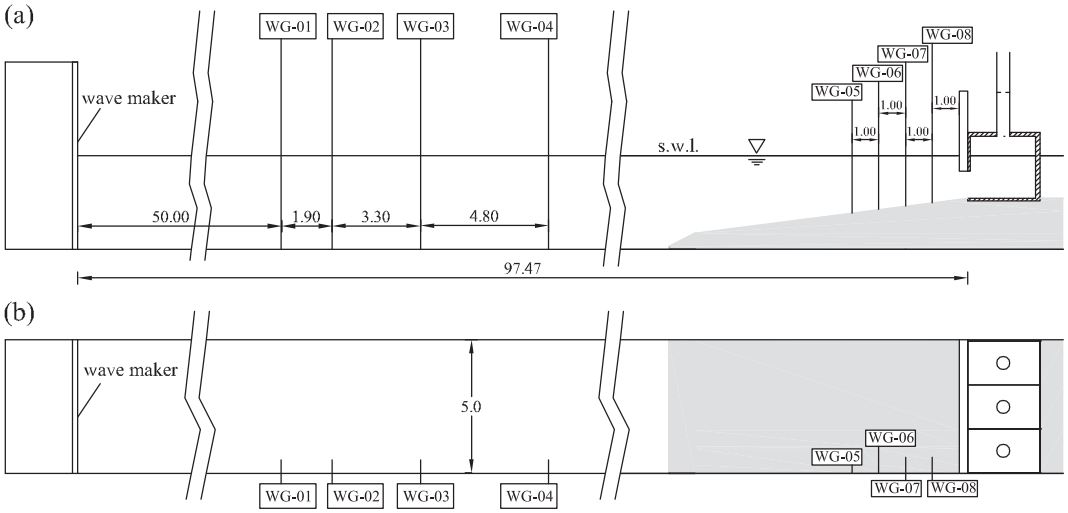

Fig. 2. Experimental setup at GWK with indication of wave gauges along the channel: (a) longitudinal section; (b) top view. All dimensions in m.

Table 2
Tested conditions, obtained by varying: orifice diameter (d_0), peak period (T_p) and nominal significant (spectral) height ($H_{m0,i}$) of incident random waves at the wave maker, still water depth at the wave maker (h), draft of caisson front vertical wall (a).

Test number	d_0 [m]	T_p [s]	$H_{m0,i}$ [m]	h [m]	a [m]
1; 2; 3; 4; 5	0; 0.05; 0.1; 0.2; 0.3	3.0	0.26	3.5	0.58
6	0.2	3.0	0.39	3.5	0.58
7; 8	0; 0.2	3.0	0.52	3.5	0.58
9; 10; 11; 12	0.05; 0.1; 0.2; 0.3	4.0	0.40	3.5	0.58
13; 14	0; 0.2	4.0	0.60	3.5	0.58
15	0.2	4.0	0.80	3.5	0.58
16; 17	0; 0.2	4.5	0.26	3.5	0.58
18; 19; 20; 21; 22	0; 0.05; 0.1; 0.2; 0.3	5.0	0.54	3.5	0.58
23	0.2	5.0	0.81	3.5	0.58
24; 25	0; 0.3	6.0	0.67	3.5	0.58
26	0.2	6.0	1.00	3.5	0.58
27	0.2	6.5	0.40	3.5	0.58
28	0.2	3.0	0.26	3.0	0.08
29	0.2	3.0	0.52	3.0	0.08
30	0.2	4.0	0.60	3.0	0.08
31	0.2	5.0	0.54	3.0	0.08
32	0.2	6.0	0.67	3.0	0.08

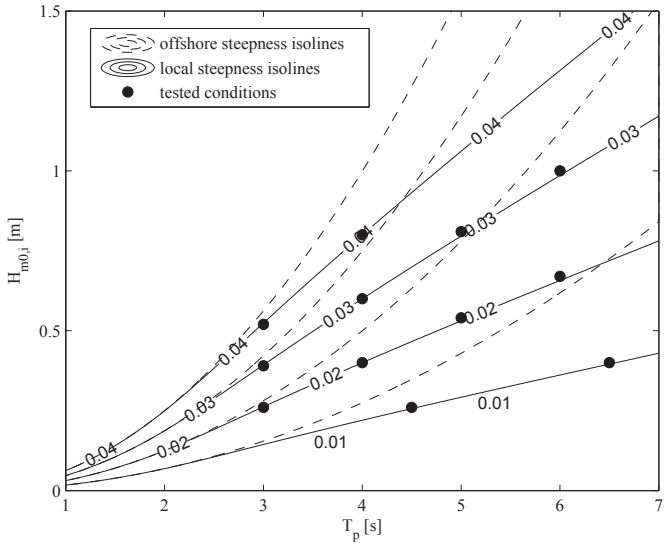

Fig. 4. Nominal wave characteristics ($H_{m0,i}$ and T_p) of the tested conditions on lines of constant offshore and local wave steepness; local wave steepness is calculated at depth $h = 3.5$ m, by applying dispersion relation.

was 0.2 m, and this value was adopted as a standard for the remaining tests. More details on the wave reflection as function of orifice diameter are reported in Section 3.2.

3. Wave reflection

A mutual influence is expected to exist between wave motion and OWC: i) a reduction on wave reflection is expected, with respect to vertical wall breakwaters, since the OWC device is able to convert incident wave energy into (ultimately) kinetic energy of air passing through the orifice; ii) the intensity of wave reflection will have some influence (probably complicated) on the loading of the OWC caisson both on its front face and within the chambers. Wave motion dynamics, addressed in this Section, is preliminary to the loading aspects which are explored in Section 4. In particular, the objective here is the wave reflection estimation as function of: incident wave characteristics, OWC caisson dimensions and air flux restriction due to the orifice.

3.1. Estimation of reflected waves

Wave motion at the wave flume can be separated into incident and reflected components using simultaneous free surface elevations at several wave gauges. The experimental set-up at GWK allowed the use of up to four wave gauges (WG01-WG04) placed in the flat bed zone of the channel, well offshore of the foreshore and OWC. For this reason, an advanced method has been adopted for wave reflection estimation [38] which makes use of data from all the four wave probes. Such a method extends the widely used Mansard and Funke three-probe formulation [39], which is in turn based on the Goda and Suzuki two-probe approach [40]. In detail, the wave field is assumed to be the sum of linear incident and reflected wave components and can be expressed in complex form as follows:

$$\eta = \sum_{n=-N}^{N} \left[f_{In} e^{i(\omega_n t - k_n x)} + f_{Rn} e^{i(\omega_n t + k_n x)} \right], \text{ for } n \neq 0 \tag{1}$$

where: t is the time variable; x is the direction of incident wave propagation; subscript n is representative of the nth harmonic component; $\omega_n = 2\pi n / t_{end}$ is the discrete angular frequency, where t_{end} is the total duration of data to be considered; k_n is the wave number obtained from the linear dispersion relation as function of ω_n and water depth. f_{Rn} and f_{In} are two complex parameters, defined respectively for reflected and incident waves, whose absolute values are the amplitudes and their arguments represent the phases.

The Fourier transformation, applied at each probe m, allows the wave signal η_m to be written as a function of a complex parameter $F_{n,m}$, defined generally for the mth probe and nth harmonic component:

$$\eta_m = \sum_{n=-N}^{N} F_{n,m} e^{i\omega_n} \tag{2}$$

Moreover, from eq. (1), it is possible to obtain:

$$F_{n,m} = f_{In} e^{-ik_n x_m} + f_{Rn} e^{ik_n x_m} \tag{3}$$

where x_m is the position of each probe m; the origin of the x abscissa can be placed at the wave probe nearest to wave-maker ($m = 1$), in such a way that x_m represents the distance between the general probe and the first one (and consequently $x_1 = 0$).

eq. (3) can be applied to each probe to obtain, for the generic nth harmonic, a system of m linear equations in which f_{In} and f_{Rn} are the only unknowns. If $m = 2$, i.e. only two probes are used, such a system can be easily solved since it is composed by two equations and two unknowns. The determinant of such a system vanishes for $x_2/L_n = 0.5$. Therefore, to obtain reliable results using this method, the ratio x_2/L_n should be in the range of $0.05 - 0.45$. This limitation is important, especially for random waves, because it is not easily satisfied for each component of the spectrum. If $m > 2$, least square method can be used and the results are more stable, also for random waves.

Absolute values of f_{In} and f_{Rn} are proportional to incident and reflected wave amplitudes of the nth harmonic, respectively. Thus the spectral reflection coefficient $C_{r(f)}$, related to the angular wave frequency component ω_n, and the total reflection coefficient C_r of a random wave train can be computed, respectively, as follow:

$$C_{r(f)} = \frac{|f_{Rn}|}{|f_{In}|} \tag{4}$$

$$C_r = \sqrt{\frac{\sum_{n=n_1}^{n_2} \left|f_{Rn}\right|^2}{\sum_{n=n_1}^{n_2} \left|f_{In}\right|^2}} \tag{5}$$

where n_1 and n_2 are, respectively, the lower and upper bounds of the spectral range used to compute the reflection coefficient.

The formulation summarized above is described in detail in Ref. [38], in which it was applied for $m = 2;3;4$, i.e. for two, three and four wave probes. The finding was that three- and four- probe methods yield similar values, but the four-probe method reduces the effect of measurement errors with respect to the more familiar three- probe method, proposed in Ref. [39]. The two probe method produces a false reflection coefficient when the wave spectrum frequency range is wide, so is not considered further here.

The cited methods for wave reflection estimation have been applied here for the analysis of wave motion in front of the OWC device described in Section 2. The results for three- and four- probe methods are shown in Fig. 5 for all the tests carried out. Wave length L_p is estimated by means of dispersion relation for peak wave period T_p and still water depth h at the wavemaker. It can be noted that the results from three- and four- probe methods provides reflection coefficient values which range between 0.4 and 0.9. Generally these two methods give most similar values of reflection coefficient. The four- probe method gives most reliable values [38]. Thus only the four-probe method results are considered in the remaining part of this paper.

3.2. Reflection coefficient

The estimation of total reflection coefficient, for all the random wave tests, allows the study of the effect of the geometric parameters varied in the experiments, i.e. orifice diameter and still water depth. In the present analysis, two dimensionless parameters which affect the wave motion have been identified in order to maximize the applicability of the experimental results to other OWC configurations having similar shape.

As regards the orifice dimension, it is possible to note that the air flows in the OWC system are forced by changes in free surface elevation inside the chamber and constrained by the orifice restriction. Since the flow is regulated by the orifice area, the orifice diameter (d_0) has been replaced, in the following analysis, by the relative orifice surface area defined as the ratio between orifice area and chamber's horizontal cross-sectional area:

$$A_0/A_c = \frac{\pi(d_0/2)^2}{BB_t} \tag{6}$$

Such a dimensionless parameter, obtained on the basis of the system geometries defined in Table 1, ranges between 0 and 2% for the configurations tested at GWK, as it is summarized in Table 3.

Still water depth variation may affect wave-air dynamics at OWC by means of the draft (a) of the frontal "curtain" wall. Thus the draft can be related to the still water depth at the OWC entrance (d) by introducing a dimensionless parameter a/d which represents the relative draft of the frontal wall.

Both dimensionless parameters A_0/A_c and a/d, related to surface orifice and frontal wall draft respectively, have been used in Fig. 6 for the analysis of total reflection coefficient as function of relative caisson width (B/L_p). As regards the orifice influence on wave motion, it is no surprise that the reflection coefficient is near to 0.9 when the air conduct is closed, i.e. $A_0/A_c = 0$, in agreement with the formulation proposed in Ref. [41] for plain vertical wall demonstrating that the OWC chambers do not dissipate wave energy when air does not flow into or out of the device.

For non zero values of orifice area, the total reflection coefficient decreases. In particular, Fig. 6(a) shows that the reduction of reflection coefficient is evident even for the smallest non zero value of relative surface orifice, i.e. $A_0/A_c = 0.1\%$. As expected, the behaviour of reflection coefficient is not monotonic with respect to orifice dimensions: it decreases until relative surface orifice is equal to 0.9%, after that an increase of wave reflection effect is noticeable, for $A_0/A_c = 2\%$.

The efficiency of the OWC device (i.e. chamber air energy over incident wave energy) and the reflection coefficient are strictly related to each other. They have an opposite behaviour, as it is possible to demonstrate on the basis of energy balance arguments, see for example Tseng et al. [28]. As a consequence, an optimized orifice opening is believed to give both the maximum energy conversion efficiency and minimum wave reflection.

The effect of orifice variation on OWC efficiency has been investigated by Thiruvenkatasamy & Neelamani [42] and, more recently, by Ashlin et al. [43]. In both studies the optimum

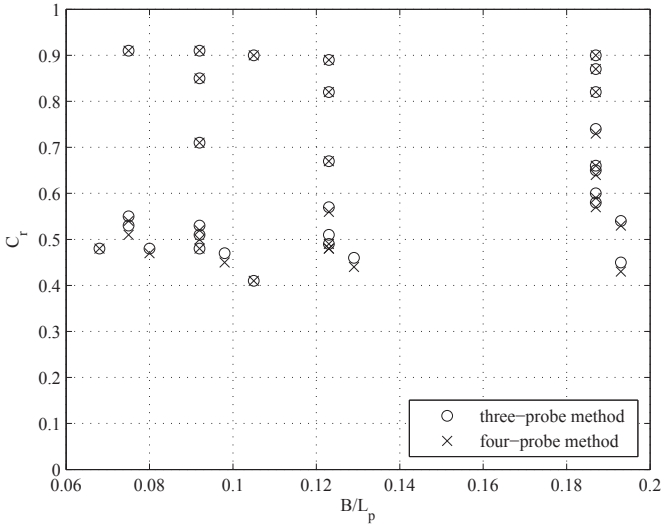

Fig. 5. Evaluated reflection coefficients C_r, in front of OWC device, as function of relative chamber width B/L_p. The circle and cross symbols denote results of three- and four-probe methods respectively. Clusters of circles and crosses indicate that three- and four-probe methods are working similarly.

Table 3
Dimensionless parameter for the tested conditions: relative orifice surface area A_0/A_c, with of caisson over peak wave length B/L_p, significant incident relative wave height $H_s^* = H_{m0,i}/h$, relative draft of frontal wall a/d.

Test number	A_0/A_c [%]	B/L_p	H_s^*	a/d
1; 2; 3; 4; 5	0; 0.1; 0.2; 0.9; 2.0	0.19	0.07	0.37
6	0.9	0.19	0.11	0.37
7; 8	0; 0.9	0.19	0.15	0.37
9; 10; 11; 12	0.1; 0.2; 0.9; 2.0	0.19	0.11	0.37
13; 14	0; 0.9	0.19	0.17	0.37
15	0.9	0.12	0.23	0.37
16; 17	0; 0.9	0.12	0.07	0.37
18; 19; 20; 21; 22	0; 0.1; 0.2; 0.9; 2.0	0.12	0.15	0.37
23	0.9	0.12	0.23	0.37
24; 25	0; 2.0	0.11	0.19	0.37
26	0.9	0.09	0.29	0.37
27	0.9	0.09	0.11	0.37
28	0.9	0.09	0.09	0.07
29	0.9	0.07	0.17	0.07
30	0.9	0.07	0.20	0.07
31	0.9	0.07	0.18	0.07
32	0.9	0.07	0.22	0.07

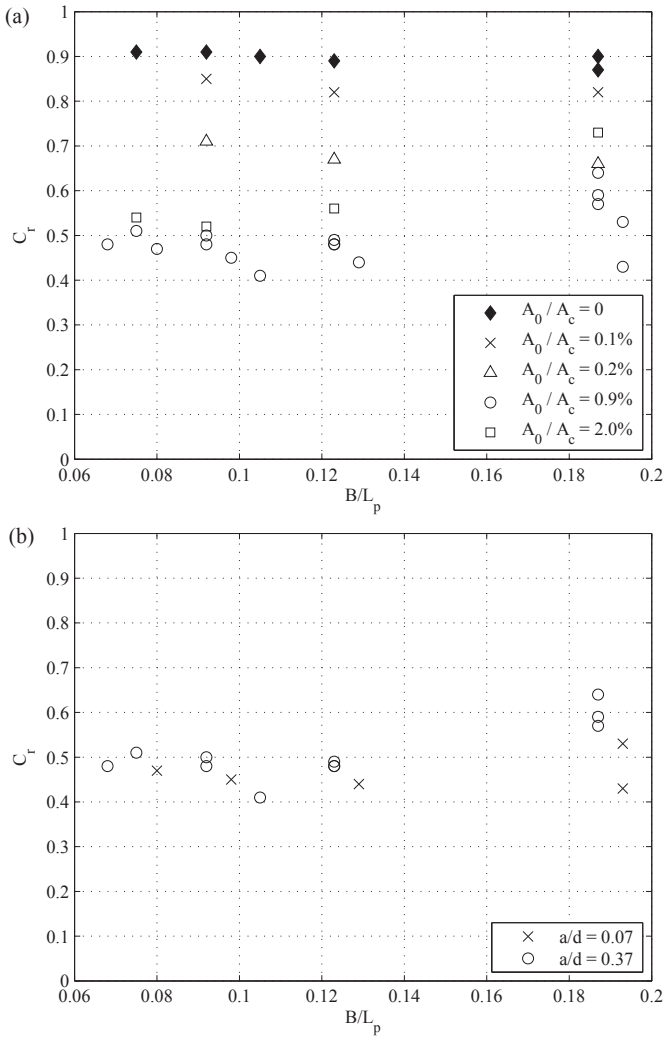

Fig. 6. Reflection coefficients C_r as function of relative chamber width B/L_p: (a) influence of orifice relative area A_0/A_c; (b) influence of relative draft of frontal wall a/d, for $A_0/A_c = 0.9\%$.

dimensionless orifice opening, which gives the greatest efficiency, ranges between 0.6% and 0.9%. Such values are similar to the optimum orifice obtained here, again minimizing wave reflection.

The physical meanings of these optimum values are related. In detail, the damping at the orifice is higher for any opening smaller than the optimum, causing greater absolute values of relative air pressure (in both compression and decompression steps) and smaller water surface oscillations into the chamber, so leading to a reduction of efficiency, as reported in Ashlin et al. [43]. The increase of wave reflection for opening smaller than the optimum is also due to the greater air pressure inside the chamber, which reaches its maximum for closed orifice.

If an orifice opening is greater than its optimum, Thiruvenkatasamy & Neelamani [42] found that the absolute values of relative air pressure decrease so causing reduction of efficiency, notwithstanding the increase of free surface oscillation inside the chamber. Such a higher free surface oscillation causes the increase of wave reflection seen in these GWK tests.

Since the wave reflection is inversely related to the efficiency of the system in converting wave energy, the value 0.9% of relative surface orifice represents an optimum in this OWC device's characteristics. For this reason, the $A_0/A_c = 0.9\%$ configuration has been studied more fully, as can be seen in Fig. 6(a) and in Table 2.

The behaviour of reflection coefficient, as function of relative width of the caisson, shows an inverse relation for smallest values of non-zero orifice dimension, i.e. for $0 < A_0/A_c \leq 0.2\%$. When the orifice opening is equal or greater than its optimum value ($A_0/A_c = 0.9\%$), a proportional relationship can be seen between C_r and B/L_p for relative width greater than 0.11. Between these, a marginally reduced reflection coefficient is observed for values of relative width near to 0.11.

A focus on C_r behaviour for the optimum orifice is shown in Fig. 6(b) by varying the draft of the front wall. Reflection coefficients are slightly lower for small drafts, particularly evident for $B/L_p > 0.11$, i.e. for the shortest waves. The physical explanation may be related to the fact that the shorter period waves have orbital velocities which decrease most rapidly toward the bottom.

Thus the lower the front wall (and thus the smaller the opening), the less intense is the wave motion into the OWC caisson, and the greater the reflected wave height. When however the front wall is shallow, and the opening greatest, then the reflection coefficient may increase as the incident waves act more on the rear wall. Such results can be used for the validation of boundary conditions in depth integrated numerical models for wave propagation [47,48].

The influence of incident wave characteristics on wave motion reflected by the OWC device has been studied by means of the spectral reflection coefficient $C_{r(f)}$, defined for each wave frequency f. Fig. 7(a) shows the effects of peak wave period variation, through the relative width of caisson calculated using the peak wave length (B/L_p). For each frequency component, the spectral reflection

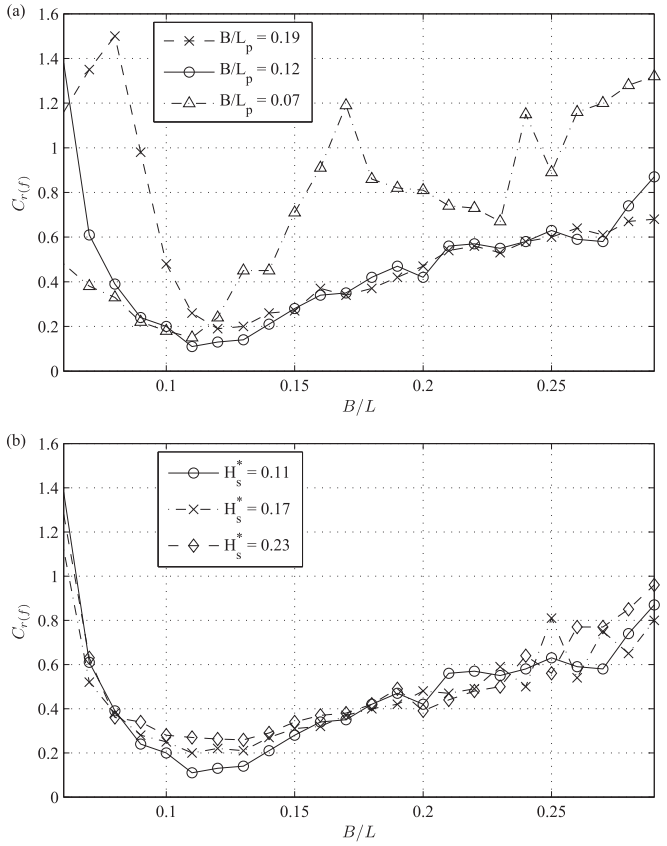

Fig. 7. Spectral reflection coefficients $C_{r(f)}$ as function of B/L of each frequency component: (a) influence of peak wave period by means of peak relative width of caisson B/L_p for tests (n. 6, 11 and 27) with relative incident wave height $H_s^* = H_{m0,i}/h = 0.11$; (b) influence of relative incident wave height H_s^* for tests (n. 11, 14 and 15) with relative chamber width $B/L_p = 0.12$.

coefficient, $C_{r(f)}$, is plotted against the relative chamber width B/L, for that frequency component's wavelength L at water depth h from the flume floor. In Fig. 7(a) all data have a fixed significant incident relative wave height $H_s^* = H_{m0,i}/h = 0.11$, such that the influence of peak wave length upon $C_{r(f)}$ is isolated. This value for H^* has been selected since it represents a median value between those tested, for which wave breaking does not take place. It is possible to observe that all the spectral reflection coefficients approach their minimum values, for $0.10 < B/L < 0.15$, relatively independently of the characteristics of incident waves. This agrees with results of physical modelling of breakwaters with perforated caisson having non-homogeneous porosity [e.g. Refs. [38,44].

In the rest of the domain, the function $C_{r(f)}$ is more influenced by the relative width of caisson B/L_p. For each B/L_p a different maximum is found, with apparent values of reflection greater than 1. Such 'unphysical' behaviour may be an indication of energy transfer between wave frequencies. Since wave energy conversion in the OWC system is related to both water and air motion, air flowing through the orifice is influenced by compression and hydrodynamics. In particular, the air flowing through the orifice (PTO) represents an oscillating motion which is the result of compression and expansion of air inside the chamber. Its behaviour is similar to a spring oscillating with a frequency which depends upon its geometry and the actions applied to it, i.e. the wave motion. The variation in time of wave characteristics in random waves influences the frequency of air intake and outflow. Air compressibility acts like a filter on the wave frequencies which are converted into air flow cycle frequencies. When the incident wave at OWC is not in phase with the air in/out flow, the air instantaneously adjusts its pressure and more slowly adjusts its frequency. The waves having near dominant (peak) frequencies are converted into air flow, thus they are partly absorbed by the system. On the contrary, several incident waves are unable to enter into the OWC since they are not in phase with the air motion. In the worst case, waves are in phase with pressure variation, thus retrieving pressure energy stored in the air chamber and not yet converted into air kinetic energy. For such frequencies, the amplitude of reflected wave component is greater than the incident one and the spectral coefficient $C_{r(f)}$ is greater than 1. As a consequence, the possibility of obtaining reflected waves greater than incident waves is strictly related to the possibility of storing energy inside the caisson by means of air pressure potential energy.

The behaviour of spectral reflection coefficient for fixed $B/L_p = 0.12$ and variable H_s^* is shown in Fig. 7(b): the minimum values of $C_{r(f)}$ increase proportionally with H_s^* and they vary between 0.1 and 0.3. However the shapes of the $C_{r(f)}$ versus B/L distribution are quite similar to each other, indicating a relatively weak influence of wave height. Since non-linearity is often related to wave height, this last finding indicates that the air-water dynamics at the OWC can probably be linearized and can be related to wave period and chamber dimensions.

The low reflection coefficient obtained for the optimum orifice allows to consider the OWC integrated into breakwaters as a good alternative to Jarlan-type breakwaters. Further discussions on waves reflection at the OWC are reported in the last Section of the paper.

4. Loadings

4.1. Data analysis

Pressure transducers were installed in the OWC caisson to measure loadings on the front wall, on the rear wall and in the ceiling (see Fig. 3). Each transducer is logged at a frequency of 1000 Hz in order to adequately describe impulsive loadings. Forces on the caisson have been computed by integrating pressure on the three surfaces with transducer arrays. In particular, the force at the front wall has been obtained by considering only the wet surface. The height of such a wet surface has been linearly extrapolated on the basis of the free surface elevations measured at the two wave gauges nearest to the front wall. At the top of that wall the (relative) pressure is assumed to be zero. At the bottom of the front wall, and at all the corners of the two internal walls (i.e. roof and rear wall), the pressures have been assumed to be equal to that registered by the nearest pressure sensor. In such a way the pressures are defined along each wall in which pressure sensors are located. The force at each wall is computed as the sum of the trapezoid areas delimited by the linear pressure distributions along that wall, multiplied by the transverse width of the OWC.

At negative pressures, and immediately around the moment of zero down crossing, the pressure signals exhibited an unphysical oscillation (see for example the time series shown in Fig. 8). A filter has been developed and applied which acts only when loads downcross the zero value for more than one time-step. Thus, the maximum actual peaks have not been modified by filtering procedure because they are always surrounded by positive values.

The pressure-time signals have been truncated with the removal of the early part until such time as the wave conditions are properly established. The time of the signal, taken into account for the following data analysis, corresponds to a nominal 1000 waves for each probe. Maximum loadings have been computed by establishing the four maximum values of the forces at the wall, the averages of which give the 1/250 forces. Values of the circumscribing

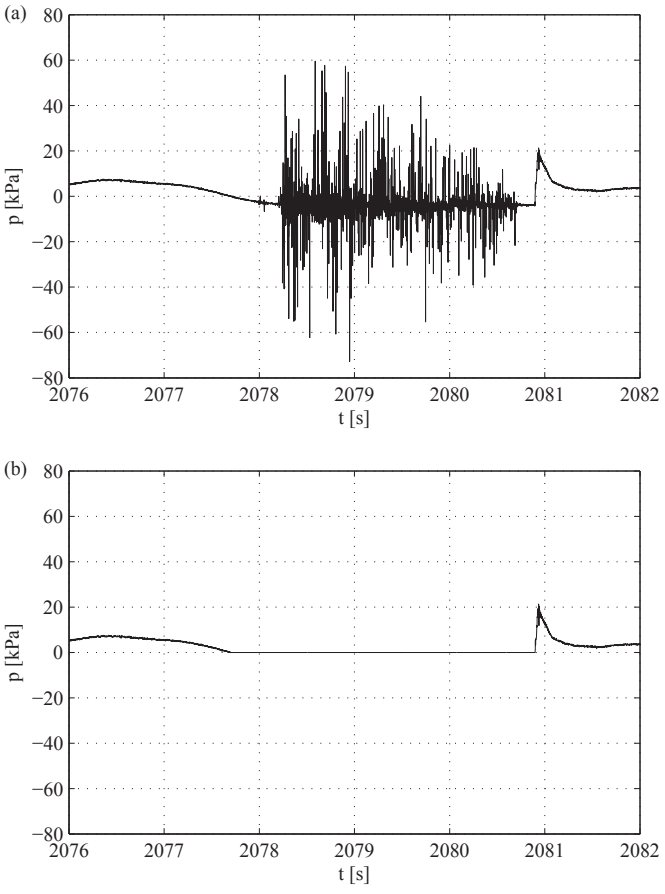

Fig. 8. Pressure signal registered by transducer n.1, placed on fontal wall at height 3.09 m from the bottom of the channel. Test condition n.26: $T_p = 6.0$ s, $H_s = 1.0$ m, $d_0 = 0.2$ m; (a) unfiltered signal; (b) filtered signal.

1/250 pressures have been computed by extracting for each transducer the 4 values corresponding to the 4 largest wave forces. This procedure yields maximal values for the 1/250 pressure distributions.

In this approach however, the maximum loadings on each wall are not extracted at the same instant; so the maximum values of force (and pressures) at each wall may be related to different waves or to different phases of the same wave.

4.2. Pressures

The results of the procedure to identify 1/250 pressures at the OWC caisson are here analyzed by considering the dimensionless pressure $p/(\rho g H_{m0,i})$ and the dimensionless axes x/B and z/d. Such analysis is focused on the widely tested optimum orifice $A_0/A_c = 0.9\%$.

The maximum (1/250) pressure distribution on the external front wall is reported in Fig. 9. It is compared with the 'extended Goda' formulation [45] for impulsive loadings on plain vertical walls.

Both the influence of wave period and wave height are considered, by means of parameters B/L_p and $H_s^* = H_{m0,i}/h$, respectively. In all the tests, the measured pressure distributions are similar to that computed, with the peak value located near the still water level, i.e. at $z/d = 0$. The match with Goda predictions is quite good for small wave heights, $H_s^* = H_{m0,i}/h \leq 0.11$, with a slight over-prediction of pressures by the 'extended Goda' formulation. As wave heights increase, the pressure peak is shifted upwards, as is shown in Fig. 9(b).

Such behaviour is not captured by the 'extended Goda' formulation, which therefore under-estimates pressures for $z/d > 0$. On the contrary, the pressures under the still water level give slightly lower values than predicted. The 'extended Goda' formulation cannot be compared with measured pressure data for $z/d \leq -0.4$ because in this point the pressure drops to zero due to the presence of the frontal wall opening.

Measured pressure distributions (1/250) inside the caisson, on the rear wall are illustrated in Fig. 10 for varying peak wave length and incident wave height. Such distributions have been compared with a formulation developed by Takahashi & Shimosako [46] for loadings within a perforated wall caisson. Notwithstanding some evident geometrical differences between OWC and perforated caissons, predicted distributions are qualitatively similar to those measured inside the OWC caisson: the pressures increase from the bottom and reach a maximum near the still water level, after which they reduce towards the roof. For lower wave heights, pressures

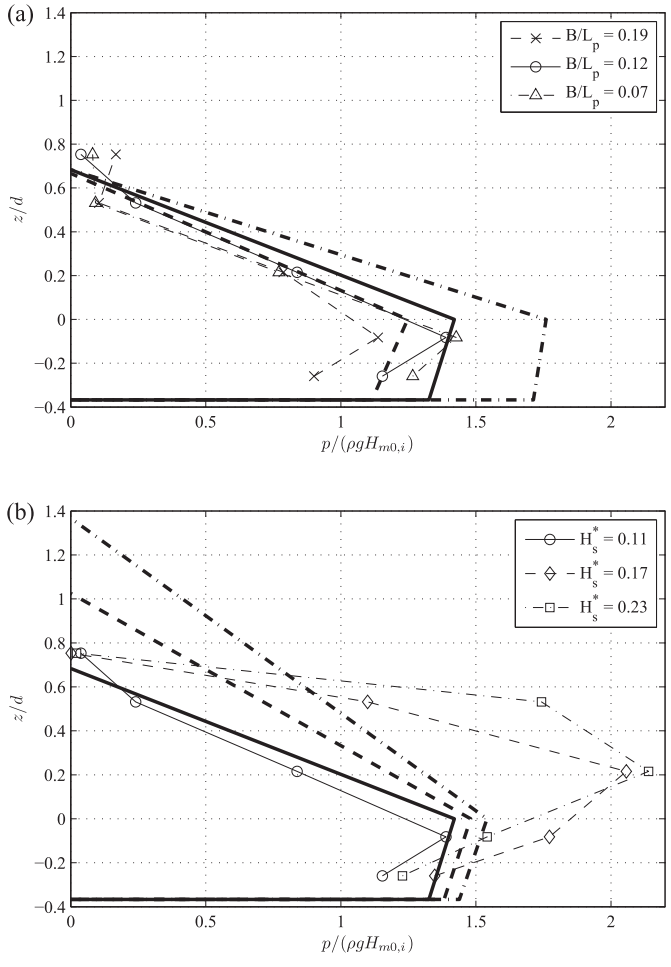

Fig. 9. Recorded and estimated maximum dimensionless pressure (1/250) on the front wall; pressures recorded by transducers are reported in markers; results of 'extended Goda' formulation [45] are shown in thick lines (without markers), having the same hatch of the measured pressures: (a) influence of peak wave period by means of B/L_p (dash line: 0.19, continuous line: 0.12, dash-dot line: 0.07) for fixed $H_s^* = H_{m0,i}/h = 0.11$; (b) influence of relative incident wave height H_s^* (continuous line: 0.11, dash line: 0.17, dash-dot line: 0.23) for $B/L_p = 0.12$.

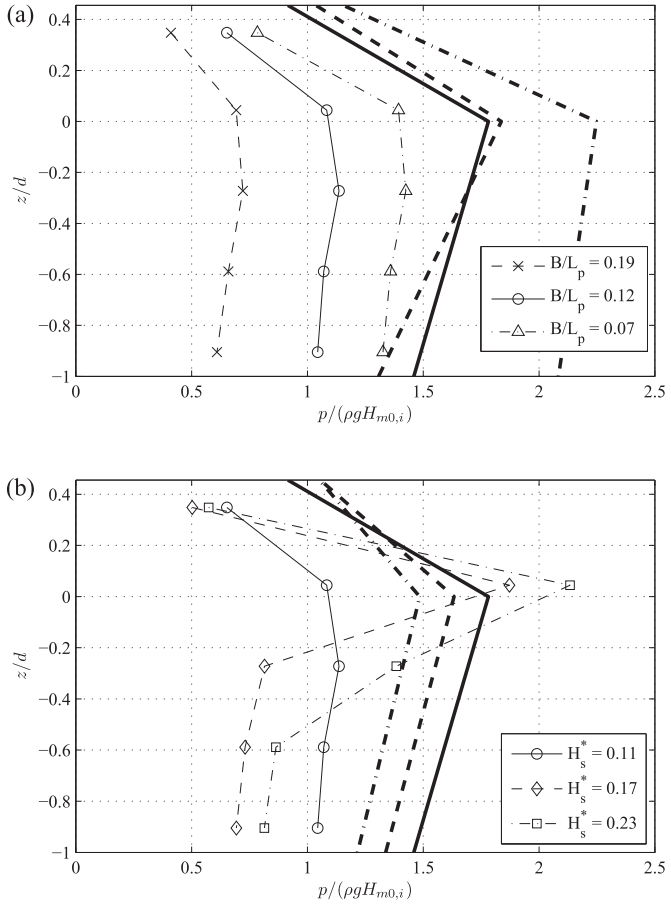

Fig. 10. Maximum dimensionless pressure (1/250) distributions on the rear vertical wall; results of perforated wall caisson Takahashi & Shimosako formulation [46] are shown in thick lines; (a) influence of peak wave period by means of B/L_p (dash line: 0.19, continuous line: 0.12, dash-dot line: 0.07) for fixed $H_s^* = H_{m0,i}/h = 0.11$; (b) influence of relative incident wave height H_s^* (continuous line: 0.11, dash line: 0.17, dash-dot line: 0.23) for $B/L_p = 0.12$.

measured on the rear wall of the OWC chamber are generally smaller than might be predicted. Conversely, for more impulsive wave conditions, $H_s^* \geq 0.17$, pressures at or above the static water level exceed predictions. The pressures are similar to those measured on the front wall for the same wave conditions.

Finally the pressure distribution on the chamber ceiling, reported in Fig. 11, show a uniform shape for non-impulsive wave conditions ($H_s^* = 0.11$). The pressures measured in these cases are therefore of the air, compressed in the upper part of the chamber. Fig. 11(a) shows that these pressures are little influenced by wave period, and are inversely related to B/L_p.

If the incident wave height increases, a peak of pressure is encountered at the rear corner of the roof, as it is shown in Fig. 11(b). This is probably caused by a jet on the rear wall hitting the chamber roof. It is important to highlight that the width of the jet is not caught by the available experimental data. Pressures measured on the rest of the roof are lower than those obtained for non-impulsive waves. It is likely therefore that this jet is related to instabilities in the OWC chamber that do not significantly pressurise air in the chamber, so may adversely affect the efficiency as a WEC.

The presence of jet inside the chamber has been observed during the tests and it would probably cause problems to any air turbine.

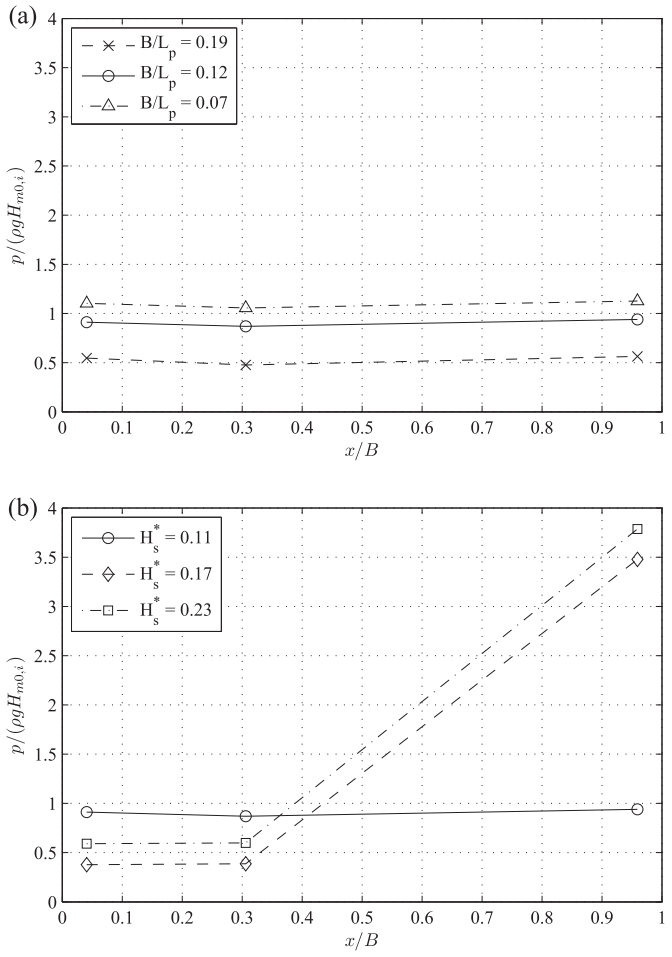

Fig. 11. Maximum dimensionless pressure (1/250) distribution at the roof of the caisson, obtained from pressure sensors P6, P13 and P7, placed at $x/B = 0.04$, 0.31 and 0.96 respectively; (a) influence of peak wave period by means of peak relative width of caisson B/L_p for fixed $H_s^* = H_{m0,i}/h = 0.11$; (b) influence of relative incident wave height H_s^* for $B/L_p = 0.12$.

4.3. Forces

Measured maximum forces, defined as 1/250 of the peak forces acting on the OWC caisson, are analyzed here for all the random wave conditions tested. The effects of incident wave height and of orifice opening have been investigated by means of the dimensionless parameters H_s^* and A_0/A_c, respectively.

Measured forces on the frontal wall have been compared with forces predicted by the 'extended Goda' method for vertical walls [45], as for the pressure distribution discussed previously. Fig. 12 shows the ratio between measured and predicted forces as function of relative wave height, for all the orifice openings tested. The horizontal solid line represents exact agreement between measured and predicted forces: the points below such a line correspond to over-predicted cases; the points above the line are unsafe, since the adopted formulation gives lower values of force with respect to those measured.

The results suggest that the maximum forces are inversely related to orifice opening. The relative error is below 40% when $H_s^* < 0.2$, independent of orifice opening. In particular, Goda formulation overestimates the measured force for $H^* = 0.11$ ($F_{measured}/F_{predicted} < 1$), i.e. for low impulsive waves. Such a behaviour is in accordance to what shown in Fig. 9(b), where the pressures measured are always lower than Goda prediction for $H^* = 0.11$. When H^* increases the pressure overcomes the Goda predictions since impulsive effects are more intense. For $0 < H^* < 0.11$ Fig. 12 shows a decrease of the ratio $F_{measured}/F_{predicted}$ as function of H^* which does not correspond to a decrease of force (and/or pressure): it is only an underestimation of the Goda formula, which is probably related to the reduction of scale effects in large wave flume (GWK), compared to Goda experiments. However the pressures and forces at the front wall always increase with H^*, as it is physically expected.

When the relative wave height increases, $H_s^* > 0.2$, forces increase and the simplified predictions become unsafe.

As regards the internal rear vertical wall, the ratio between measured and predicted force is shown in Fig. 13, using the perforated caisson prediction method by Takahashi & Shimosako [46]. The forces are generally inversely related to orifice opening, with the exception of a case for which relative incident wave height

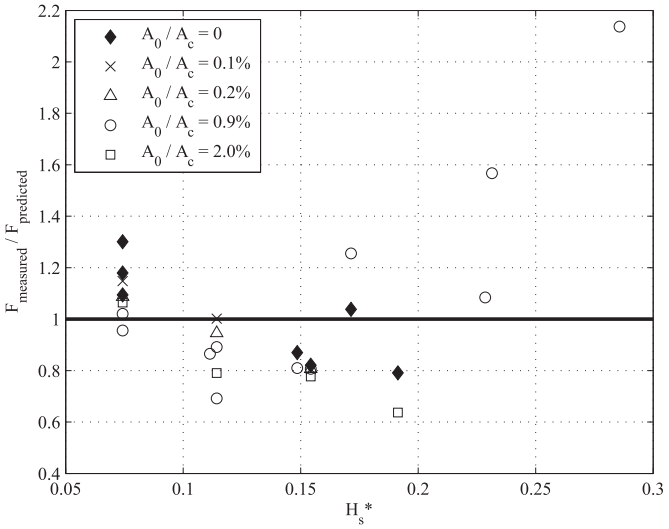

Fig. 12. Ratio between measured and predicted forces (1/250) at the external frontal wall, by applying the 'extended Goda' formulation [45]. Influence of relative incident wave height ($H_s^* = H_{m0,i}/h$) and of orifice surface ratio A_0/A_c. Solid line represents the best mean fit.

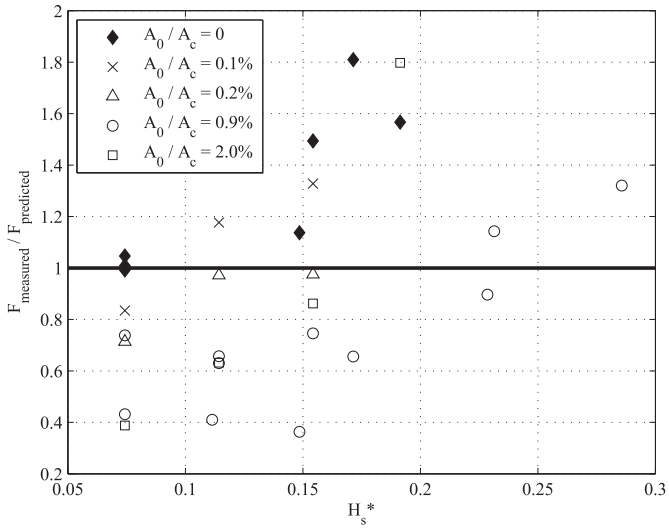

Fig. 13. Ratio between measured and predicted forces (1/250) at the internal rear wall, by applying the perforated wall caisson formulation [46]. Influence of relative incident wave height ($H_s^* = H_{m0,i}/h$) and of orifice surface ratio A_0/A_c. Tick line represents the best fit, the points over such a line are unsafe with the adopted formulation.

is near to 0.18. It is noted that the method adopted was not developed for OWC caissons. Even so, the method generally gives greater predicted forces than those measured, particularly for optimum orifice ($A_0/A_c = 0.9\%$). On the contrary, loads on the rear wall are greater for orifice openings smaller or larger than the optimum.

Dimensionless forces on the ceiling of the chamber at 1/250 level are shown in Fig. 14, suggesting general increases with increasing relative wave height H_s^*. An optimum orifice opening appears to lead to significantly lower internal loadings relative to those measured for smaller or larger orifices.

It is worth highlighting that the maximum dimensionless force is measured under conditions with the largest orifice, rather than under closed orifice conditions. The likely explanation is that under the closed orifice conditions, there is little movement of the water inside the chamber, mitigating strongly against the formation of the type of jet responsible for the much larger rear-wall and chamber ceiling pressures and forces. It is clear however that conditions that

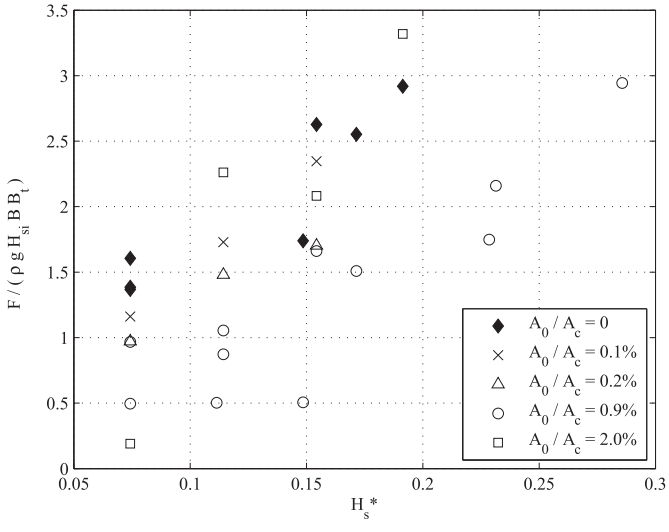

Fig. 14. Measured dimensionless maximum forces (1/250) at the roof. Influence of relative incident wave height ($H_s^* = H_{m0,i}/h$) and of orifice surface ratio A_0/A_c.

lead to pulsating motions within the OWC chamber therefore pressurise the air in the chamber relatively uniformly. Conversely, conditions that cause sloshing within the chamber are more likely to give rise to impacts on the rear wall and on the ceiling of the chamber.

5. Conclusions

The aim of this work is to provide useful information contributing to the design of OWC systems integrated into vertical breakwaters, with particular attention to wave reflections and loadings on the front wall, rear wall, and on the ceiling of the chamber. The results obtained allow the consideration of the OWC breakwater as a possible alternative to composite and perforated caissons to reduce reflections which affect the classic vertical wall breakwaters. In such a context the energy production is a complementary aspect and will be addressed in future publication, by considering the complex interaction between air flow and a power take off (PTO).

Large scale experiments in the GWK, carried out under random wave conditions, have explored the effects of: orifice restriction (i.e. PTO); water depth, and wave conditions on wave motion, by means of suitably defined dimensionless variables.

In detail, relative orifice area affects significantly the total reflection coefficient which reaches a maximum, equals $C_r \approx 0.9$, when the orifice is closed. This agrees with the literature for reflection of random waves from vertical walls. Moreover the minimum of reflection is not reached for the largest tested orifice but for an optimum condition. For tests reported here, this optimum was found when the relative orifice surface is equal to 0.9%, from which reflection coefficient $C_r \approx 0.5$. Such an orifice maximises the capacity of the system to convert wave energy into air kinetic energy.

The variation of still water depth, for fixed OWC geometry, affects wave motion by means of draft variation of the frontal wall: reflection coefficient is found to increase with wall draft and, consequently, with still water depth.

The influence of incident significant wave height and peak wave period on both spectral reflection coefficient and pressure distribution have been investigated. It has been found that all the spectral reflection coefficients reach a minimum when the relative width of the caisson chamber $B/L \approx 0.10 - 0.15$. This agrees with physical models results for non-homogeneous perforated wall breakwater.

The OWC system presents similar aspects to Jarlan-type breakwaters. Such analogy has been verified also in the loading estimation, indeed a formulation has been considered for prediction of pressure distribution inside the caisson which was developed for perforated breakwater. It has been shown that the predicted shape of pressure distribution is qualitatively similar to that measured along the rear vertical wall, i.e. the maximum pressure is located near the still water level.

The loading measured on the frontal external wall, compared with the 'extended Goda' formulation for vertical wall, shows differences less than 40% when the relative wave height $H_s^* \leq 0.2$. After that the error increases and the considered formulation becomes unsafe.

Measurements of pressure on the ceiling of the caisson give uniform values for low significant wave heights and a spike at the rear corner for the highest incident waves. This last behaviour is related to the presence of a jet within the chamber, caused by a breaking wave which impacts the real wall, as observed by the internal camera during testing. Such jets may cause problems to air turbine that may be installed at the OWC. Thus, a system have to be introduced for deflecting these upwards jets away from the air duct

to the turbine. The OWC turbine should to be closed when near breaking wave conditions appear, both for the safety of the chamber structure and of the turbine.

Acknowledgments

The authors are grateful to HR Wallingford, the University of Edinburgh, Second University of Naples, Queen's University of Belfast, University of East Anglia for supporting the staff time devoted to this project. Access to the GWK has been supported by European Community's Seventh Framework Programme through the grant to the budget of the Integrating Activity HYDRALAB IV within the Transnational Access Activities, Contract no. 261520. The authors would also like to thank Dr Matthias Kudella and Dr Stefan Schimmels and their support team at the GWK for their cheerfulness, tolerance and considerable assistance in the design evolution, model construction, and testing. Important input from Professor Trevor Whittaker (Queen's Belfast) and Dr Mark Cooker (Univ. East Anglia) in the study design is gratefully acknowledged. Assistance in the testing and supporting physical and numerical modelling from Nic Miller and David Bourke (University of Edinburgh), Mariangela Sfouni-Grigoriadou, Encarnacion Median-Lopez, Giovanni Cuomo, Aggelos Dimakopoulos and Daniele Longo (HR Wallingford), Vincenzo Ferrante (Second University of Naples) is also gratefully acknowledged.

References

[1] R.A. Arinaga, K.F. Cheung, Atlas of global wave energy from 10 years of reanalysis and hindcast data, Renew. Energy 39 (1) (2012) 49–64, http://dx.doi.org/10.1016/j.renene.2011.06.039.
[2] K. Gunn, C. Stock-Williams, Quantifying the global wave power resource, Renew. Energy 44 (2012) 296–304, http://dx.doi.org/10.1016/j.renene.2012.01.101.
[3] F. Arena, V. Laface, G. Malara, A. Romolo, A. Viviano, V. Fiamma, G. Sannino, A. Carillo, Wave climate analysis for the design of wave energy harvesters in the Mediterranean Sea, Renew. Energy 77 (2015) 125–141, http://dx.doi.org/10.1016/j.renene.2014.12.002.
[4] D. Vicinanza, P. Contestabile, V. Ferrante, Wave energy potential in the north-west of Sardinia (Italy), Renew. Energy 50 (2013) 506–521, http://dx.doi.org/10.1016/j.renene.2012.07.015.
[5] C. Iuppa, L. Cavallaro, D. Vicinanza, E. Foti, Investigation of suitable sites for wave energy converters around Sicily (Italy), Ocean Sci. 11 (4) (2015) 543–557, http://dx.doi.org/10.5194/os-11-543-2015.
[6] M. Monteforte, C.L. Re, G. Ferreri, Wave energy assessment in Sicily (Italy), Renew. Energy 78 (2015) 276–287, http://dx.doi.org/10.1016/j.renene.2015.01.006.
[7] A.F. Falcao, Wave energy utilization: a review of the technologies, Renew. Sustain. Energy Rev. 14 (3) (2010) 899–918, http://dx.doi.org/10.1016/j.rser.2009.11.003.
[8] K. Koca, A. Kortenhaus, H. Oumeraci, B. Zanuttigh, E. Angelelli, M. Cantù, R. Suffredini, G. Franceschi, Analysis of wave reflection from wave energy converters installed as breakwaters in harbour, in: Proceedings of the 10th European Wave and Tidal Energy Conference, 2013.
[9] B. Zanuttigh, E. Angelelli, G. Bellotti, A. Romano, Y. Krontira, D. Troianos, R. Suffredini, G. Franceschi, M. Cantù, L. Airoldi, F. Zagonari, A. Taramelli, F. Filipponi, C. Jimenez, M. Evriviadou, S. Broszeit, Boosting blue growth in a mild sea: analysis of the synergies produced by a multi-purpose offshore installation in the northern adriatic, Italy, Sustainability 7 (6) (2015) 6804–6853, http://dx.doi.org/10.3390/su7066804.
[10] S. Takahashi, Hydrodynamic characteristics of wave-power-extracting caisson breakwater, in: Twenty-First Coastal Engineering Conference; Costa del Sol, Malaga, Spain, 1988, pp. 2489–2503.
[11] S. Takahashi, H. Nakada, H. Ohneda, M. Shikamori, Wave power conversion by a prototype wave power extracting caisson in sakata port, in: Proc. of 23rd International Conference on Coastal Engineering, ASCE, New York, 1992, pp. 3440–3453.
[12] V. Raju, S. Neelamani, Concrete caisson for a 150 kW wave energy pilot plant: design, construction, and installation aspects, in: Proc of 2nd Int. Offshore and Polar Eng. Conf, 1992, pp. 584–591.
[13] C.B. Boake, T.J.T. Whittaker, M. Folley, H. Ellen, Overview and initial operational experience of the LIMPET wave energy plant, in: 12th International Offshore and Polar Engineering Conference, Kyushu, Japan, vol. 1, 2002, pp. 586–594.
[14] P. Boccotti, On a new wave energy absorber, Ocean Eng. 30 (2003) 1191–1200.
[15] C. Patterson, R. Dunsire, S. Hillier, Development of wave energy breakwater at Siadar, Isle of Lewis, in: Proc. Coasts, Marine Structures & Breakwaters, Thomas Telford, London, 2009, pp. 738–749.
[16] Y. Torre-Enciso, I. Ortubia, L.L. de Aguileta, J. Marqus, Mutriku wave power plant: from the thinking out to the reality, in: Proc 8th European Wave and Tidal Energy Conf, 2009, pp. 319–329. Uppsala, Sweden.
[17] Y. Torre-Enciso, J. Marqus, L.L. de Aguileta, Mutriku. Lessons learnt, in: 3rd Int. Conf. on Ocean Energy, Bilbao, 2010.
[18] F. Neumann, I.L. Crom, Pico OWC - the frog prince of wave energy? recent autonomous operational experience and plans for an open real-sea test center in semi-controlled environment, in: Proceedings of the 9th European Wave and Tidal Energy Conference (EWTEC 2011), 2011. Southampton, UK.
[19] F. Arena, A. Romolo, G. Malara, A. Ascanelli, On design and building of a U-OWC wave energy converter in the Mediterranean Sea: a case study, in: Proceedings of the 32nd International Conference on Ocean, Offshore and Arctic Engineering OMAE2013, 2013. Nantes, France.
[20] M. Buccino, D. Banfi, D. Vicinanza, M. Calabrese, G.D. Giudice, A. Carravetta, Non breaking wave forces at the front face of seawave slotcone generators, Energies 5 (2012) 4779–4803, http://dx.doi.org/10.3390/en5114779.
[21] D. Vicinanza, J.H. Nørgaard, P. Contestabile, T.L. Andersen, Wave loadings acting on overtopping breakwater for energy conversion, J. Coast. Res. Spec. Issue 65 (2013) 1669–1674.
[22] D. Vicinanza, P. Contestabile, J.H. Nørgaard, T.L. Andersen, Innovative rubble mound breakwaters for overtopping wave energy conversion, Coast. Eng. 88 (2014) 154–170.
[23] M. Buccino, D. Vicinanza, D. Salerno, D. Banfi, M. Calabrese, Nature and magnitude of wave loadings at seawave slot-cone generators, Ocean Eng. 95 (2015) 34–58, http://dx.doi.org/10.1016/j.oceaneng.2014.11.038.
[24] M. Buccino, D. Stagonas, D. Vicinanza, Development of a composite sea wall wave energy converter system, Renew. Energy 81 (2015) 509–522, http://dx.doi.org/10.1016/j.renene.2015.03.010.
[25] E. Medina-Lopez, W. Allsop, A. Dimakopoulos, T. Bruce, Conjectures on the failure of the owc breakwater at mutriku, in: Coastal Structures, 2015, p. 12.
[26] A.F. Falcao, J.C. Henriques, Oscillating-water-column wave energy converters and air turbines: a review, Renew. Energy 85 (2016) 1391–1424 doi: j.renene.2015.07.086.
[27] G. Muller, T.J. Whittaker, Visualisation of flow conditions inside a shoreline wave power-station, Ocean Eng. 22 (6) (1995) 629–641, http://dx.doi.org/10.1016/0029-8018(94)00032-3.
[28] R.-S. Tseng, R.-H. Wu, C.-C. Huang, Model study of a shoreline wave-power system, Ocean Eng. 27 (8) (2000) 801–821, http://dx.doi.org/10.1016/S0029-8018(99)00028-1.
[29] B. Zanuttigh, L. Margheritini, L. Gambles, L. Martinelli, Analysis of wave reflection from wave energy converters installed as breakwaters in harbour, in: Proceedings of the 8th European Wave and Tidal Energy Conference, 2009, pp. 384–392.
[30] R. Curran, T.P. Stewart, T.J.T. Whittaker, Design synthesis of oscillating water column wave energy converters: performance matching, Proceedings of the Institution of Mechanical Engineers, Part A, J. Power Energy 211 (6) (1997) 489–505, http://dx.doi.org/10.1243/0957650981537375.
[31] I. Lopez, B. Pereiras, F. Castro, G. Iglesias, Optimisation of turbine-induced damping for an OWC wave energy converter using a RANS-VOF numerical model, Appl. Energy 127 (2014) 105–114, http://dx.doi.org/10.1016/j.apenergy.2014.04.020.
[32] Y.-S. Kuo, C.-S. Lin, C.-Y. Chung, Y.-K. Wang, Wave loading distribution of oscillating water column caisson breakwaters under non-breaking wave forces, J. Mar. Sci. Technol. 23 (1) (2015) 78–87, http://dx.doi.org/10.6119/JMST-014-0114-1.
[33] M. Sainflou, Essai sur les digues maritimes verticales. (test on vertical sea dikes), Ann. des Ponts Chaussees 98 (1928) 5–48.
[34] Y. Goda, A new method of wave pressure calculation for the design of composite breakwaters, in: Proceeding of the Port and Harbour Research Institute, Ministry of Transport, Nagase, Yokosuka, Japan, 1973, pp. 41–69.
[35] S.J. Ashlin, S.A. Sannasiraj, V. Sundar, Wave forces on an oscillating water column device, Proced. Eng. 116 (2015) 1019–1026, http://dx.doi.org/10.1016/j.proeng.2015.08.336, 8th International Conference on Asian and Pacific Coasts (APAC 2015).
[36] W. Allsop, T. Bruce, J. Alderson, V. Ferrante, V. Russo, D. Vicinanza, M. Kudella, Large scale tests on a generalised oscillating water column wave energy converter, in: Proceedings of the HYDRALAB IV Joint User Meeting, Lisbon, 2014.
[37] J.W. Weber, Representation of non-linear aero-thermodinamic effects during small scale physical modemodel of OWC WECs, in: Proceeding of the 7th European Wave and Tidal Energy Conference, 2007.
[38] C. Faraci, P. Scandura, E. Foti, Reflection of sea waves by combined caissons, J. Waterw. Port, Coast. Ocean Eng. 141 (2) (2015) 04014036, http://dx.doi.org/10.1061/(ASCE)WW.1943-5460.0000275.
[39] E. Mansard, E. Funke, The measurement of incident and reflected spectra using a least squares method, in: Proc. 17th Int. Coastal Engineering Conf, ASCE, New York, 1980, pp. 154–172.
[40] Y. Goda, Y. Suzuki, Estimation of incident and reflected waves in random wave experiments, in: Proc. 15th Int. Conf. Coastal Engineering, ASCE, New York, 1976, pp. 828–845.
[41] W. Allsop, W. McBride, D. Colombo, The reflection performance of vertical walls and low reflection alternatives: results of wave flume tests, in:

Proceedings of Thr 3rd MCS Project Workshop, MAS2-CT92-0047, Monolithic (Vertical) Coastal Structures, De Voorst, The Netherlands, 1994.
[42] K. Thiruvenkatasamy, S. Neelamani, On the efficiency of wave energy caissons in array, Appl. Ocean Res. 19 (1997) 61–72, http://dx.doi.org/10.1016/S0141-1187(97)00008-4.
[43] S.J. Ashlin, V. Sundar, S. Sannasiraj, Effects of bottom profile of an oscillating water column device on its hydrodynamic characteristics, Renew. Energy 96 (Part A) (2016) 341–353, http://dx.doi.org/10.1016/j.renene.2016.04.091.
[44] K.J. McConnell, N.W.H. Allsop, D.M. Ethelston, Wave reflection from coastal structures: development and application of new approaches, in: Proceeding of the 10th Congress of Asia and Pacific Division of IAHR, 1996.
[45] S. Takahashi, K. Tanimoto, K. Shimosako, A proposal of impulsive pressure coefficient for design of composite breakwaters, in: Proc. of International Conference on Hydro-technical Eng. for Port and Harbor Construction, Port and Harbour Res. Inst, 1994.
[46] S. Takahashi, K. Shimosako, Wave pressure on a perforated wall, in: Proc. of International Conference on Hydro-technical Eng. for Port and Harbor Construction, Port and Harbour Res. Inst, 1994.
[47] C. Lo Re, R.E. Musumeci, E. Foti, A shoreline boundary condition for a highly nonlinear boussinesq model for breaking waves, Coast. Eng. 60 (2012) 41–52.
[48] A. Viviano, R.E. Musumeci, E. Foti, A nonlinear rotational, quasi-2DH numerical model for spilling wave propagation, Appl. Math. Model. 39 (2015) 1099–1118.